Dark Current Measurements of a Multicell, 805 MHz Cavity

J. Norem
HEP Division, Argonne National Laboratory, Argonne IL 60439

V. Wu
University of Cincinnati, Cincinnati OH 45221

A. Moretti, M. Popovic, Z. Qian
Fermi National Accelerator Laboratory, Batavia IL 60510

L. Ducas
University of Illinois, Urbana, IL 61801

Y. Torun, N. Solomey
Illinois Institute of Technology, Chicago, IL 60616
(Apr. 17, 2002)

Measurements of dark currents and x rays in a six cell 805 MHz cavity are presented. We compare our data with other measurements from a variety of different accelerating structures. We also describe production mechanisms and discuss the degree to which emitter parameters are experimentally accessible. Dark currents are involved with the limitations on the gradients that can be produced in a wide range of particle accelerator structures. The electric fields reached were large enough to mechanically damage emitter surfaces.

I. INTRODUCTION

The problem of operating single particle detectors in the presence of rf cavities, with the immediate goal of an experimental demonstration of muon cooling, has directed interest in the study of dark currents and the x rays they produce [1] [2] [3]. While dark current phenomena are almost universally seen in accelerating structures, there has been comparatively little systematic study of the basic mechanisms with realistic copper accelerating structures. Our goal is to develop 200 MHz high gradient cavities, and the primary problem is the emission of dark currents which cause backgrounds in our detectors and breakdown in the cavities. We have used an 805 MHz cavity (Fig 1), to help understand the phenomena involved in dark current emission and transport [4] [5]. The accelerating field for this π mode cavity was given by $E_{acc,[MV/m]} = \sqrt{33 P_{[MW]}}$, and the maximum surface field is 2.6 times E_{acc}.

This study uses a six cell cavity designed to accelerate muons between absorbers in a muon cooling channel [6] [7] [8]. Since a variety of solenoidal fields will be present in the cooling channel, the test cell is surrounded by a two coil superconducting magnet capable of producing either solenoidal mode, with the coils in series adding, or a gradient mode, with the coils in opposition. The magnet produces a 5T field on axis in solenoidal mode and 3.5 T maximum field in gradient mode [9].

Dark currents can be studied with a variety of approaches and techniques, all of which have some applicability to accelerator problems [10]. While DC enclosures can produce useful data, and very high frequencies are also studied, accelerating structures which operate around 1 GHz are relevant since they are comparatively easy to work with and can access the basic physics of these effects.

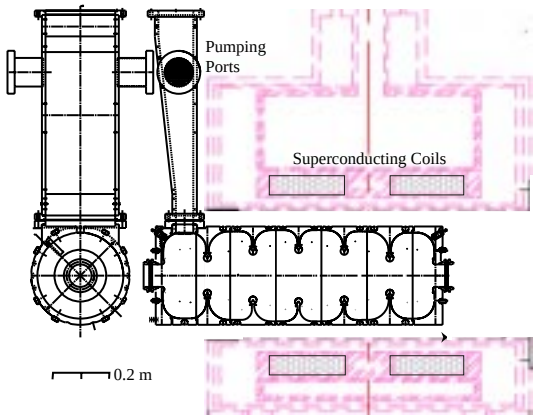

FIG. 1. The RF cavity in the superconducting magnet.

II. DARK CURRENT SOURCES

Fowler Nordheim field emission, which proceeds by quantum tunneling thru a potential barrier, is described by a current density, j, in A/m^2 given by [1],

$$j(E) = \frac{A_{FN}(\beta_{FN}E)^2}{\phi} \exp\left(-\frac{B_{FN}\phi^{3/2}}{\beta_{FN}E}\right),$$

where E is the electric field in MV/m, ϕ is the work function of the material in eV, with $A_{FN} = 1.54 \times$

10^6eVA/(MV)^2, $B_{FN} = 6830$ V/m(eV)$^{3/2}$, and β_{FN} expresses the enhancement of the local electric field at the presumably pointlike emitter, compared with the average electric field [1] [11] [12]. For all useful materials the work function is around 4.6 eV. The emitted current is then $I(E) = A_{rf} A_e j(E)$, where A_e is the total emitter area, and A_{rf}, described below, corrects for the time variation of the sinusoidal field. We plot $\log_{10} I$ vs. $\log_{10} E_{acc}$, which presents the data as a function of the measurable quantities, where the effects of the two variables, β_{FN} and A_e, are linear, simple and comparatively intuitive (Fig 2). This format also permits comparisons between data from different facilities and detectors, and can show perturbations, for example due to the $I \sim E^{3/2}$ dependence of space charge limited currents. The structure of the data makes relatively precise measurements of β_{FN} possible, but the experimental errors in determining A_e are comparatively large. Most of our data shows values $A_e \sim 10^{-12} - 10^{-14}$ m^2, which implies sub micron emitter sizes.

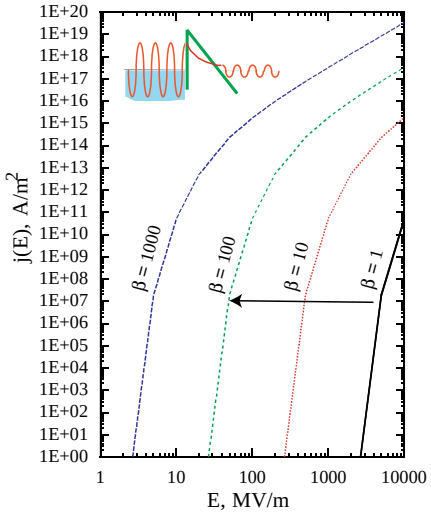

FIG. 2. Fowler Nordheim field emission

We assume that emission from a cavity is dominated by a few emitters whose local electric field is in the range 1-10 GV/m. This is because the rapid rise of current with field heavily weights the data towards the highest field emitters. We measure the sum of currents from different emitters in the cavity in a somewhat imprecise way, detecting only the fraction of the current which is emitted thru the window. The field enhancement is expected to be due to a number of factors, 1) the shape of the cavity makes the local field on the irises higher by a factor of about 2.6, 2) visible roughness such as pitting, scratches and copper beads deposited from breakdown will produce an additional factor, probably in the range of 5 - 20, and, 3) the actual emitter point seems to be sharp, considerably smaller than 1 μm, contributing another factor of perhaps 10. All of these factors are multiplied together to give the enhancement β_{FN}.

While large enhancement factors could be a function of the product of many smaller enhancements, they could be produced by single structures. For example it has been shown that a hairlike metallic protrusion with a length 100 times its diameter and a spherical end whose radius is equal to that of the hair would produce a enhancement factor roughly equal to the aspect ratio of the hair [10]. While these structures seem unlikely, we did see metallic hairs laying down on the surface with comparable dimensions, and these are described below, along with a description of mechanisms which can stand them on end.

There are other mechanisms of emission of electrons from sources, in addition to Fowler Nordheim tunneling, such as thermal emission, and emission from filaments in oxides, which will be discussed below. Thermal emission is described by the expression

$$j_{th}(T) = AT^2 e^{-\phi/k_B T},$$

where A is equal to 1.2×10^6 A/m^{2}K^2, k_B is Boltzmann's constant, equal to 8.62×10^6 eV/K, and ϕ is the work function of a few eV [13]. The expressions for thermal emission and tunneling are qualitatively similar. Emission from the two mechanisms is equal when $T \approx E/1.4$, if T and E are in units of degrees K and MV/m. Unless the emitter temperature is above 5000 °K, however, thermal emission is many orders of magnitude lower than the current density from Fowler Nordheim tunneling. Nevertheless, thermal emission may be involved more directly in breakdown, where very high densities of local heating may be found.

III. CAVITY MEASUREMENTS

A. $B_{sol} = 0$

The study of dark currents began in the middle of the conditioning procedure with measurements using a beam transformer that was read out with a Tektronix TDS 3054 oscilloscope [14] [15]. As the conditioning progressed, we extended the lower limit of current measurements by averaging up to 64 pulses to remove statistical fluctuations from the signal. Towards the end of the measurements, we also used a 100X rf amplifier with a high frequency cutoff around 10 MHz, mounted near the transformer, to improve the signal to noise ratio and permit more accurate measurements with smaller currents. The pulse shape of the dark current is shown in Fig. 3 for 19 and 29 μs pulses. Measurements of dark current were made using 19 μs pulses.

At low power the dark current pulse was approximately triangular, with a maximum at the end. At high powers saturation effects sometimes rounded off the end of the dark current pulse, causing it to turn over. A variety of effects which could contribute to saturation are described below.

Measurements of range of the dark current electrons(described below) indicate that the signal measured with a current transformer contains a significant component of Compton electrons produced from x rays. This Compton signal could consist of perhaps 5 - 10% of the direct measured dark current. This signal may be more forward peaked than the multiple scattered low energy electrons, which penetrates farther in materials.

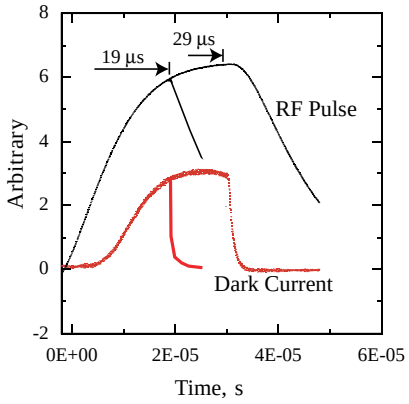

FIG. 3. Pulse shapes.

The dark current measurements are shown in Fig. 4. Measurements at the lowest current levels were made by counting the rate of electrons detected in a 0.05 m diameter x 0.025 m scintillator. Individual pulses within a 2 μs time were recorded digitally and photographically and this electron signal was converted to an instantaneous current. The first time this was tried, we found that the signal $I(E_{acc})$ was nonlinear, with a clear, narrow peak at 4.9 MV/m accelerating voltage. The next day when we repeated these measurements, the peak was not there and a simple power law dependence was observed. We assume the temporary peak was associated with multipactoring [1]. Over a limited range, $I \propto E^n$, with $9 \leq n \leq 30$.

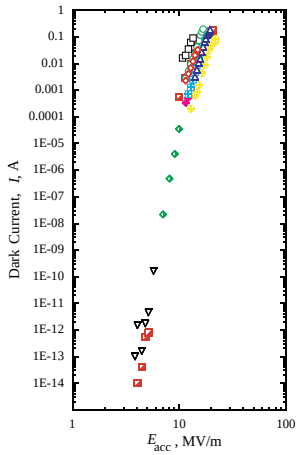

FIG. 4. Dark current measurements.

The data at intermediate voltages was taken with a SmartIon radiation meter [16]. This device was useful over about 4 orders of magnitude, but we were able to improve the dynamic range by collimating the dark current beam and renormalizing, where the data overlapped.

1. Initial Conditioning

The effect of conditioning can be seen by more closely examining the high current data, as shown in Fig. 5. There was a general trend of the $I(E_{acc})$ data set to move to higher values of E_{acc} over the first two months. The data was fitted to the Fowler Nordheim expression yielding β_{FN} and A_e. The fitted values of β_{FN} are shown in Fig. 6. The conditioning process was not smooth, and on some days the measured values of β_{FN} were higher and the conditioning was worse. During conditioning at the highest fields, the exponent n was close to 9 - 10 for weeks.

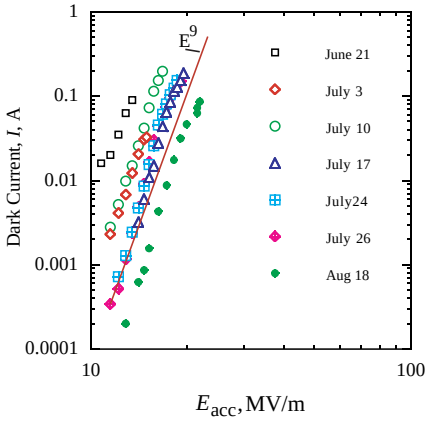

FIG. 5. High current data.

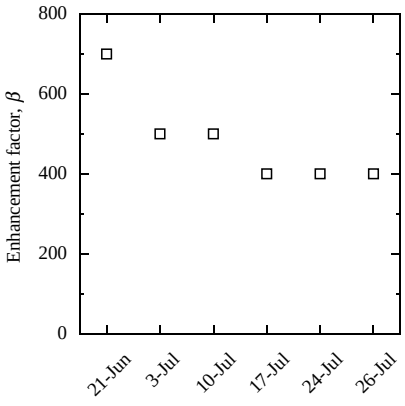

FIG. 6. Progress in conditioning.

2. Measurements of Dark Current Spectra

The dark current spectrum determines the x ray background produced. There are two important parameters: the overall shape of the electron spectrum, which determines the x ray spectrum, and the maximum energy of the electrons, which determines how efficiently the electrons will propagate through the environment. We used two methods to optimally measure both of these quantities. The overall spectrum was measured using range, and the maximum energy was measured with a magnetic spectrometer.

The magnetic spectrometer (Fig.7) was constructed using thin steel sheets and 2.54 cm thick ceramic permanent magnet material. The gap was 2.54 cm high and 5.08 cm long, and the maximum field of 0.117 T was measured along with fringe field corrections [17]. Since the magnet was so small, undeviated beam from the slit passed around the magnet and hit the Polaroid film, which permitted an accurate calibration.

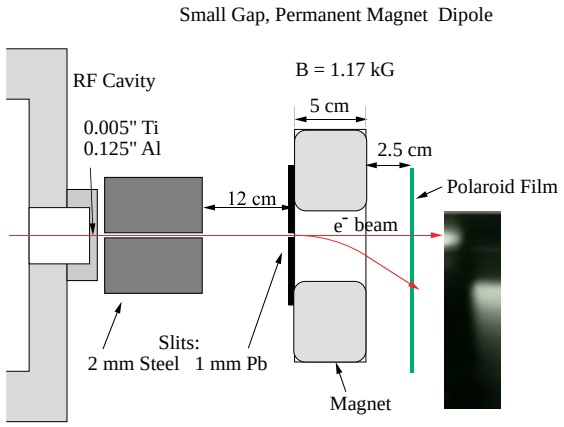

FIG. 7. The magnetic spectrometer

The spectrometer is primarily sensitive to the top end of the spectrum because, 1) the lowest momenta are bent too strongly to make it through the magnet, 2) multiple scattering at lower momenta produced a large divergence which penetrated the slit inefficiently, and 3) lower momenta come from irises close to the slit and these electrons exit the window far from the cavity axis. The spectrum produced, shown in Fig. 8, indicates that the maximum energy of the electrons is $\sim 0.5\ E_{acc}L$, where L is the length of the cavity. This roughly agrees with MAFIA calculations of electrons in the cavity, which was designed for muons moving at $\beta = 0.87$.

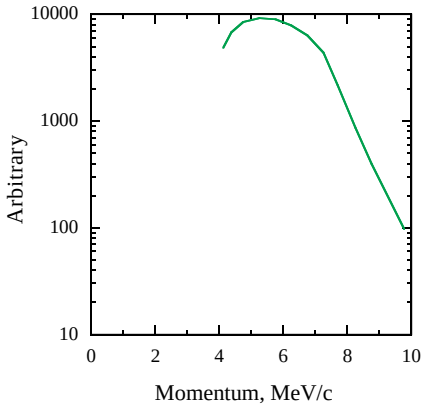

FIG. 8. Momentum spectrum from the spectrometer.

The spectra of electrons was also measured using range information in plastic, graphite and aluminum. The beam transformer was placed behind a stack of material and the current which penetrated material was plotted. This technique is described in Bethe [18]. The spectrum of electrons measured is shown in Fig. 9. We also plot the end point energy expected from 0.4 times the gradient times the cavity length. (Multiple scattering of very low energy electrons reduces the range from that expected for linear tracks.) There is a large background, presumably due to Compton x rays that penetrates the material and produces electron currents.

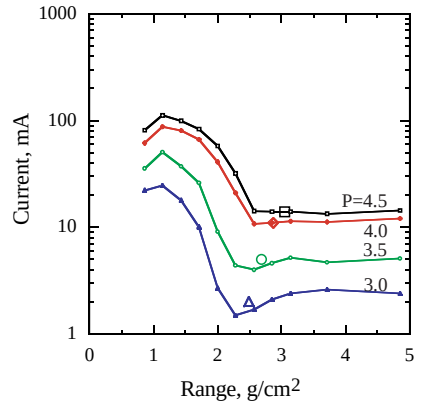

FIG. 9. Range measurements.

3. Microstructure

If emission follows a E^9 or E^{10} law, the emitted beam from an 805 MHz single cell cavity would be roughly gaussian in shape with $\sigma = 62$ ps. Since our multicell cavity is tuned for muons with a β of 0.87, and has an active length of 1 m, this narrow width could be spread by $\Delta t = (1-\beta)L/c \sim 0.5$ ns, where L is the length of the cavity and c is the speed of light.

In order to determine the microstructure of the beam, we used a coaxial Faraday cup, (shown in Fig. 10), which

had been carefully tuned to 50 Ω with a time domain reflectometer with length of low loss cable to transmit the dark current pulse to a HP 8593A Spectrum Analyzer [19]. The spectrum appeared as a series of harmonics of the 805 MHz driving frequency as shown in Fig. 11.

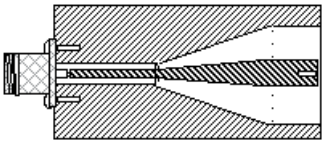

FIG. 10. The faraday cup, whose OD is 5 cm.

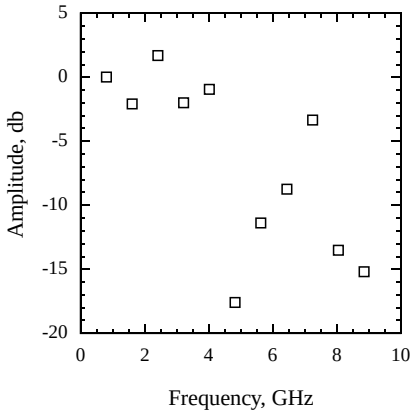

FIG. 11. The frequency spectrum

This data was then used to reconstruct the approximate shape of the pulse, assuming equal phases of the different harmonics. The result, shown in Fig. 12 is a basically rectangular pulse with a flat bottom. The FWHM of the pulse is about 200 ps, and the flat bottom is about 400 ps long.

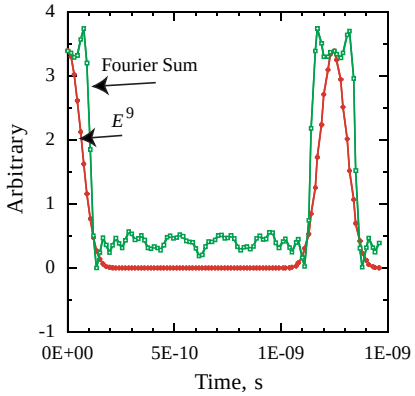

FIG. 12. The derived pulse shape.

4. Vacuum

The vacuum pressure of the cavity varied over several orders of magnitude during history of the RF processing. The vacuum pressure started at 3×10^{-6} Torr when the cavity was first turned on at 70 kW of input power, and stabilized around 2×10^{-8} Torr after 8 weeks of processing at 12 MW. When the cavity was idle (without RF input), the vacuum pressure stabilized around 5×10^{-9} Torr. During RF processing without the solenoidal field, the vacuum pressure always increased when the input power was raised. Then, after time, it stabilized to a lower pressure as a result of RF processing. The presence of the solenoidal field increased the vacuum pressure to the level of 10^{-7} Torr, an indication of enhanced outgassing. Subsequent RF processing brought the pressure back to 5×10^{-9} Torr level. The solenoid turn-on required reprocessing of the cavity as if it had never been processed before.

The vacuum pressure was monitored using a number of gauges and a residual gas analyzer, all located in the pumping port at the top of the waveguide coupler shown in Fig. 1. The partial pressures of the gasses seen are shown in Table I and Fig. 13. The base pressure measured was approximately 5×10^{-9} Torr when not pulsing. Breakdown caused the ratio of Cu/gas pressures to increase substantially, and the ratio may be even higher since copper atoms would tend to stick to the walls better than than gas atoms, and the RGA time constant is slow.

Table I, Partial Pressures, in nTorr

Mass	Gas	RF on	RF off	Breakdown
2	H_2	9.2	1.6	
16	O_2	2.5	0.4	
18	H_2O	2.4	0.4	
28	N_2/CO	6	1.8	
44	CO_2	7.8	1.4	
63	Cu	0.1	<< 0.1	0.95

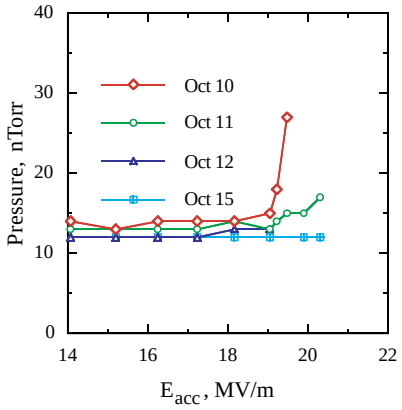

FIG. 13. Pressure as a function of acceleration field.

The surface conditions of the cavity are, to some extent, determined by its construction. This cavity was machined using a water soluble lubricant, Semcool or Holut 763, followed by cleaning with a micro degreaser, di-water rinse, alcohol rinse, Citronox rub and warm Citronox bath for 30 min, followed by another di-water rinse and alcohol rinse, after which the components were bagged in nitrogen and brazed. After brazing, all further testing and assembly was done with a nitrogen purge.

5. Nitrogen Treatment

There is a large class of discharge cleaning mechanisms which use gas in a metallic chamber. These methods presumably scrub the walls with ions which are produced with the discharge and improve the wall surface. We used nitrogen at a pressure of 10^{-5} Torr to accelerate the conditioning process. The results were obtained at the end of the run after the chamber was damaged during six months of operation, but the conditioning rate obtained was impressive, reducing the dark currents by about two orders of magnitude and increasing the accelerating voltage by a factor of about 1.25. This is shown in Fig. 14.

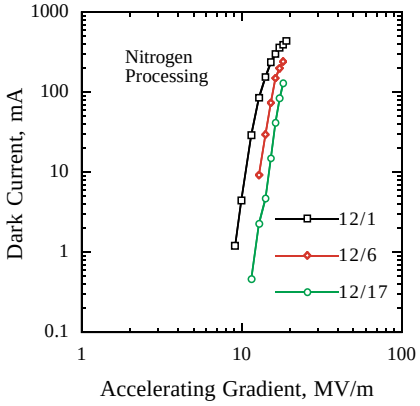

FIG. 14. Nitrogen conditioning.

B. $B_{sol} = 1 - 3$ T

The initial effect of the solenoidal magnetic field was an increase in dark currents, which required a new program of conditioning. The operation of the cavity was similar to the previous conditioning period before the magnetic field was applied. Following a conditioning process with the field on, however, the cavity operated at comparable electric field levels to those obtained with the B field off, but four times higher radiation levels were measured on axis outside the shielding. An accurate measurement of the magnetic field dependence of dark current emission after conditioning, which is one of the goals of this effort, was found to be very difficult. The fields interact with all aspects of the measurement, through the orbits of the electrons, both in and outside of the cavity, the instrumentation used, and the operation of the cavity itself.

The orbits inside the cavity, multiple scattering produced by the windows and the orbits of electrons as they leave the immediate region of the cavity, can be quite different depending on the magnetic field, and most detectors are quite sensitive to the geometrical details of the radiation flux. An additional complication is the fact that many detectors do not operate in a high magnetic fields. In addition, the magnetoresistance of the copper was seen to change the accelerating field in the cavity by about 7.5 % at 2.5 T for comparable powers, which would change the emitted current by a factor of two.

A number of methods were studied. We looked primarily at measurements of the radiation levels in the cave using radiation monitors which could see backscatter from the electrons and photons but not the cavity/magnet system itself and we also looked at radiation monitors outside the cave on the magnetic field axis. Radiation levels off-axis inside the cave, as shown in Fig. 15, showed less dependence of dark currents on magnetic field than measurements made on-axis outside the cave. Although a correction for the magnetoresistance of copper was made, both methods can be refined further.

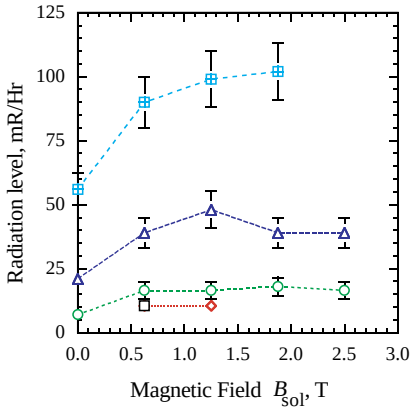

FIG. 15. Magnetic field dependence.

1. Ring Beamlets

There were two vacuum failures of the window during the conditioning of the cavity with magnetic field. When the protective cover of the window was removed, a pattern of burned spots was noted on the outside of the window, forming parts of three concentric bands. These bands seemed to be composed of a number of beamlets. Calculations of the magnetic field from the solenoid permitted the bands to be associated with the irises of the cavity, as shown in Fig. 16. We assumed that the electrons would follow the field lines to the window.

Space charge effects should determine the ultimate size of the beamlets, and these effects had a characteristic de-

pendence on B and E [20]. We then tried to measure the beamlet sizes. When glass plates were placed against the external face of the window, they showed browning from radiation damage due to the electron beam, as shown in Fig. 17. The best spatial resolution of these plates was limited by the multiple scattering in the window and was on the order of 100 μm. Since the electron energy was low, multiple scattering angles were very large. in order to keep the glass close to the concave window it was necessary to use small pieces that could only see part of the band structure. In order to look for space charge effects, we varied the electric and magnetic fields. Lowering the magnetic field to alter space charge effects, however, turned the beamlets into rings.

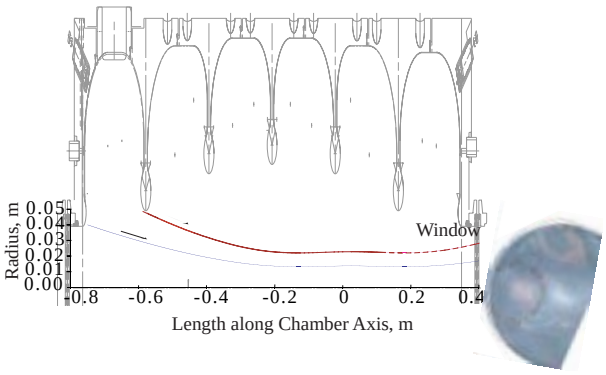

FIG. 16. The cavity geometry.

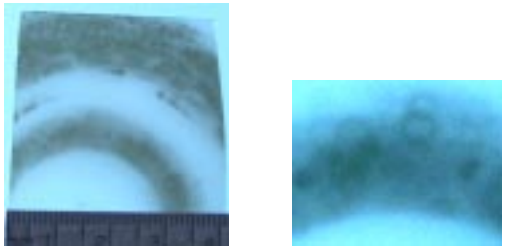

FIG. 17. The bands and beamlets in them.

The ring radius was found to be proportional to E and $1/B^2$ as shown in Fig. 18 and 19. The dynamics of these rings can be explained by $\mathbf{E} \times \mathbf{B}$ drifts during the acceleration process. As the electrons accelerate through the mostly axial magnetic field, the radial components of the electric field near the irises produce azimuthal $\mathbf{E} \times \mathbf{B}$ drifts with increasingly large radii. Since the transverse electric field components are not turned off adiabatically, the transverse momentum remains with the electrons as they are accelerated. The radii produced are roughly equal to

$$r = \frac{\gamma m_0 E_\perp}{eB^2},$$

where $E_\perp, \gamma$, m_0 and e are the component of the electric field perpendicular to the magnetic field, relativistic gamma, electron rest mass and charge. This process is commonly seen in foilless diodes and is described in reference [21].

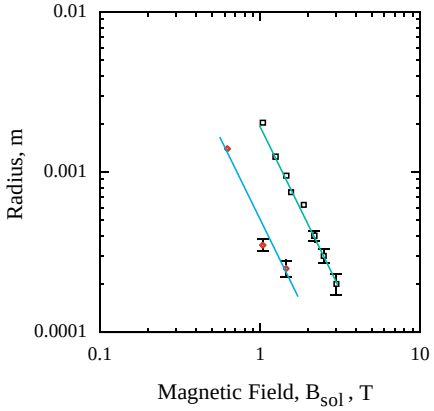

FIG. 18. Radii of beamlets as a function of solenoidal field. The upper set of data comes from the inner band.

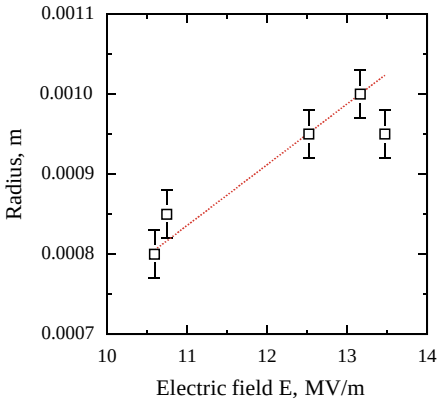

FIG. 19. Radii of beamlets in the inner band as a function of the accelerating field.

All emitters in the cavity seemed to produce ring beams, however, the diameters of the rings are dependent on the local values of E and B at the point of production. The Helmholtz coil geometry used here produced a rapidly decreasing field at the irises farthest from the coils. Since the diameters of the rings produced from the two different irises should scale like $1/B^2$, and the furthest two irises have solenoidal fields different by a factor of 2 (Fig. 20), with comparable electric fields we would expect the ring radii to be different by a factor of 4, with the outer ring producing the larger rings. This is, in fact, what is seen, as shown in Fig. 18.

The local current density may determine the power density produced when beamlets from one face of a cavity strike the opposite wall. We were unable to measure any structure with a width of less than $\sigma < 100$ μm, however this may be due to scattering in the window.

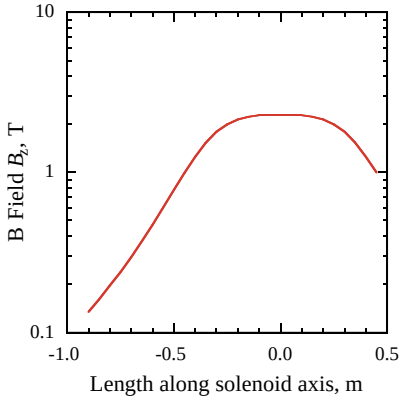

FIG. 20. Field on axis.

C. Cavity History

The initial conditioning of the cavity was performed with no magnetic field. Following the successful operation of the cavity with no field, the superconducting coils were turned on in the gradient mode at a field of 3.5 T. After a quench at this field, the magnet was operated in solenoidal mode. A window failure due to the beams of low energy electrons then caused a vacuum leak after about a month running with this field. A second period of operation with a magnetic field, during which we were able to understand the dynamics of the ring beams, also ended in window failure. The final operational period in December was devoted to nitrogen conditioning and magnet measurements. This is shown in Fig. 21. The monitor data accurately reflected the dark current intensities.

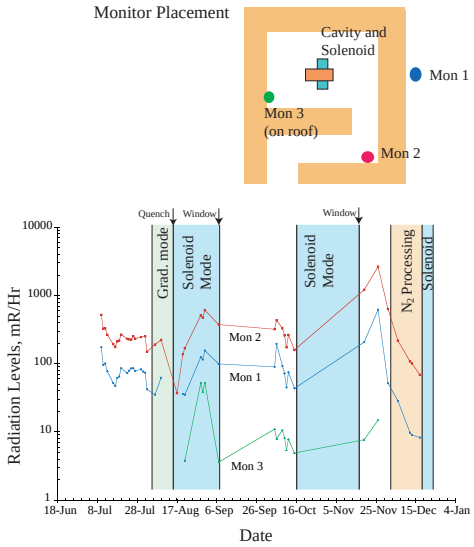

FIG. 21. The radiation history of the facility during RF processing with and without solenoidal field.

Measurements of the Q and the resonant frequency were made after the cavity was removed from the experiment. The Q was found to have changed form 15,000 to 13,500 the resonant frequency of the π mode was lowered by 13 kHz, and the frequency of the 0 mode was unchanged.

D. Window and Iris Damage

The titanium window was removed following a vacuum failure. When this window was examined two effects were noted, 1) an array of black spots on the outside of the window, and 2) copper deposition on the inside surface. In fact, the array of black spots seen on the outside of the window could also be seen on the inside, however they were partially obscured by the deposited copper.

The black dots seem to be due to field emitted electron beamlets, which heated the titanium and in a few cases melted it to cause a leak. The distribution of these spots followed the bands described in the previous section.

The black dots on the window could have been produced by local heating due to dark currents. Damage due to breakdown is also a possibility. We can examine the damage produced by the electron beams on the window using the measured beamlet diameter and the approximate magnitude of the dark currents produced by an average emitter. The titanium window will primarily be heated by dE/dx losses and the temperature rise produced will be on the order of $\Delta Q = cm\Delta T$, where c, m and ΔQ are the specific heat, mass and absorbed energy of the volume heated by the beam. Both the titanium and copper will undergo heating on the order of 30 °K/mA, so that localized beamlet currents on the order of 50 mA would be sufficient to melt the window. The time constant for the decay of this heating would be about 10-100 ms, so both long pulses and high beam currents would contribute to window damage. Microscopic examination seems to show that the copper was melted over a larger radius than the titanium, which is consistent with its lower melting point.

The copper deposited on the inside of the window seems to be produced from liquid copper droplets hitting the flat window surface and splashing. An example, somewhat larger and cleaner than most of the droplets, is shown in Fig. 22. The splash seems similar to what one obtains when liquid solder is dropped on the floor. Note that in addition to the large circular splash, there are a number of long hairlike strands visible in the picture. These hairlike strands, and the points that seem to be visible at the edge of the splatters, could produce very efficient field emission sources.

The overall distribution of copper droplets is basically smooth, with no obvious correlation with the electron produced bands described above. There is a slight increase in the density of droplets near the edges of the window, associated with a reduction in the average size,

and this might be associated with droplets bouncing off the inside of the tubes immediately in front of the window. If the particles were produced with a velocity of about 10 m/s or greater, these droplets could travel ballistically from the irises to the window with very little deflection, which would explain the even distribution of deposited copper over the area of the window.

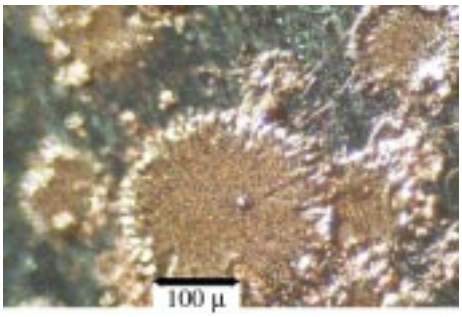

FIG. 22. Copper splattered in the inside of the window.

The copper irises were also damaged during operation. The damage occured as pitting, uniformly distributed over the surface of the high field part of the irises. The two irises near the center of the cavity were damaged more than the ones on the ends and the irises near the input coupler were damaged less than the ones at the other end. Presumably the damage is a sensitive function of the surface electric field and it is unlikely that this would be precisely equal for all 7 irises. Typical damage is shown in Fig. 23.

We have constructed a periscope/microscope which can look in detail at the spark damage on the irises of the cavity, and have begun to study the material that has been removed and transported by arcing. An image of the surface of the central iris is shown in Fig. 24. The surface shows shiny spheres of deposited copper sitting on the machined surface and a variety of other features. The size of most of these features is less than 100 μ. Small spheres deposited on large spheres could produce the enhancement factors described in Section 1.

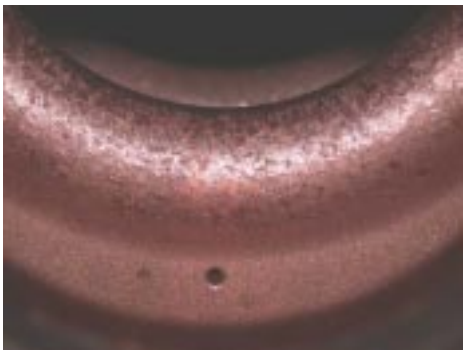

FIG. 23. Damage on the irises.

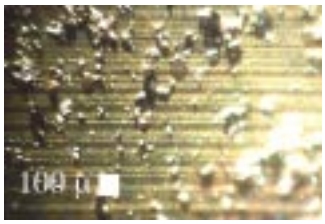

FIG. 24. A microscopic image of the center iris in the cavity.

E. Instrumentation

This paper describes measurements made on signals which vary over a wide range, in some cases fourteen orders of magnitude. A variety of techniques were used, each of which had its own limitations: beam transformers, scintillator/photomultiplier tubes, thermoluminescent detectors (TLDs), portable radiation monitors, Faraday cups, Polaroid film, personal monitoring film, area radiation monitors, glass plates, residual gas analyzers, range spectrometers, magnetic spectrometers and a variety of other standard instrumentation [22] [23]. Each of these techniques is useful over a comparatively small range of parameters. The most useful methods tend to be those in use as radiation monitors [23]. The Type 2 personal monitoring film has two emulsions and is useful over about four orders of magnitude in radiation dose, as shown in Fig. 25. Polaroid film is useful over a much narrower range, and much less radiation dose. Normal glass can be used at higher doses, but the glass fades somewhat (even in the dark) in as little as 24 hours, so the linearity is no longer useful.

We checked that different techniques for measurements tracked consistently, whenever possible. The linearity of these techniques over many orders of magnitude in signal, with the additional presence of radiation fluxes at high power levels (up to MW levels) and changing pulse shapes, was not continuously verified with high precision.

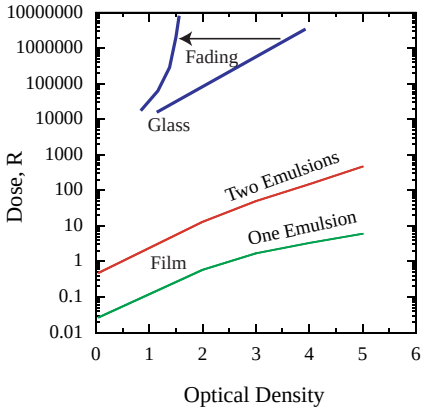

FIG. 25. Type 2 film parameters with approximate glass response curve.

IV. OTHER RECENT MEASUREMENTS

The Fowler Nordheim dependence of current on accelerating field seems to be a common feature of many types of accelerating structures. At high fields this appears as a power law dependence of the dark current, radiation level or energy loss on the electric field. At lower electric fields, the dependence of the Fowler Nordheim equation effectively increases the power law to E^{15} - E^{35}. At higher fields the dependence looks like $E^{9.6}$. This behavior seems to be a characteristic of a wide range of accelerating structures.

Both CERN superconducting rf cavities and an ANL photoinjector constructed at the Taiwan light source give radiation levels measured nearby that are proportional to $E^{9.6}$ [3]. These data are consistent with the results presented here.

Superconducting rf cavities also seem to show the same effects. The quality of superconducting cavities is described by a plot of the operating Q, a measure of the stored energy divided by loss per cycle, as a function of accelerating field [1]. Losses in a cavity, however, are more intuitively measured by $1/Q$, which is equal to the energy loss per cycle divided by 2π times the stored energy in the cavity. We have plotted these curves for a range of cavities in Fig. 26. The data are consistent with the energy loss being the sum of a constant, due to the residual resistivity ratio (RRR), and a rapidly rising loss dependent on E^n, with n in the range $n \sim 10 - 20$, see Fig. 26. We assume that this rapidly rising term is entirely due to dark current losses in the structure and have calculated the required current to generate these losses and the power law dependence on the accelerating field. When currents derived from the $1/Q$ measurements are plotted with the 805 MHz data, both show similar current levels and power law dependence, at least for the worst superconducting structures, as shown in Fig. 27. On the other hand, the best cavities, to be used in the TESLA program, operate with three times the electric field and ten orders of magnitude lower dark currents then our cavity [24].

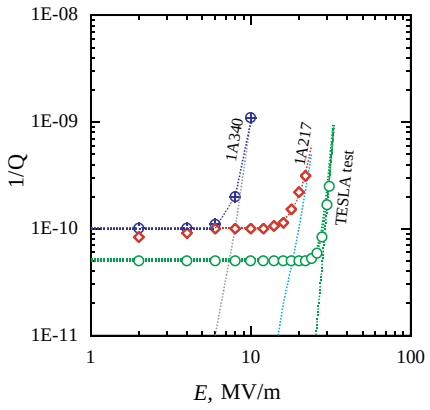

FIG. 26. SCRF cavity losses.

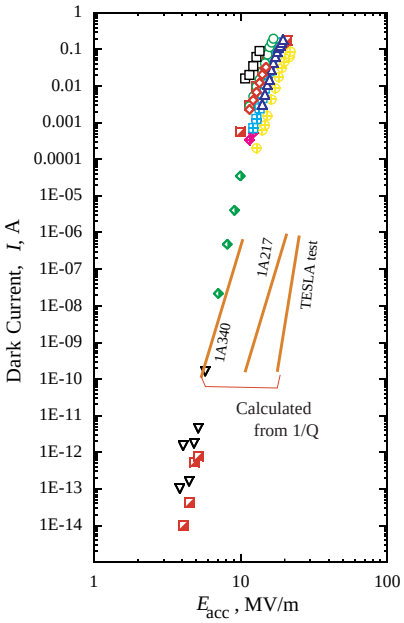

FIG. 27. SCRF dark currents compared with the 805 MHz cavity.

The very aggressive R & D effort to produce superconducting cavities which operate at higher fields has been quite successful [1] [24]. This increase was obtained primarily by means of careful attention to surface cleanliness and elimination of defects, which implies that comparable gains are possible for copper cavities.

We have also looked at x rays produced at the ISIS and IPNS proton linacs [25] [26]. These 200 MHz drift tube linacs were constructed long ago and are now the basis for pulsed neutron programs. Radiation measurements for both accelerators show that the x ray dose in the immediate region of the drift tube linacs is proportional to E^{14}, which is consistent with the power law followed in the middle region of the data shown in Figure 2. Again this seems to imply that Fowler Nordheim dark currents are the dominant mechanism. ISIS data shows an exponent n of 13.5 - 14, as shown in Fig 28.

It has been shown that x ray fluxes external to accelerating cavities with low energy electrons are primarily composed of 100 keV x rays, which are roughly isotropic [3]. The lower energy of these x rays is determined by the photoelectric effect, and their angular distribution is determined by electron multiple scattering and the Compton effect.

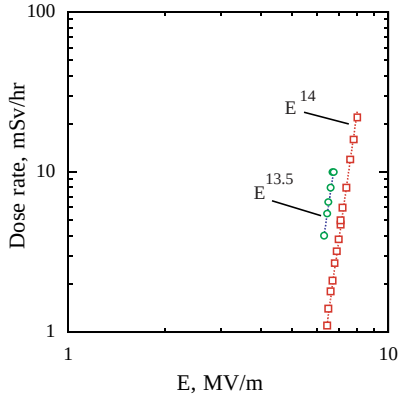

FIG. 28. Radiation levels near the ISIS linac.

Data from the IPNS linac show an E^{14} dependence of the radiation flux on the acceleration field, Fig. 29, when the radiation flux was measured about halfway down the linac tank.

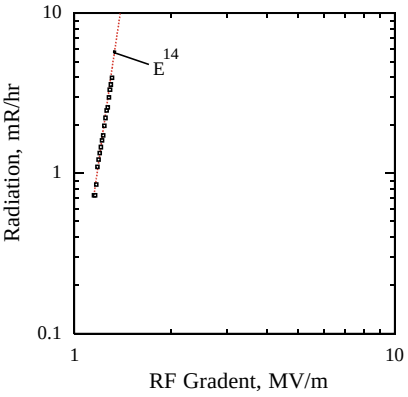

FIG. 29. Radiation fluxes near the proton linac of IPNS.

Measurements of an NLC prototype cavity show an E^{15} dependence on the field as shown in Fig. 30 [27].

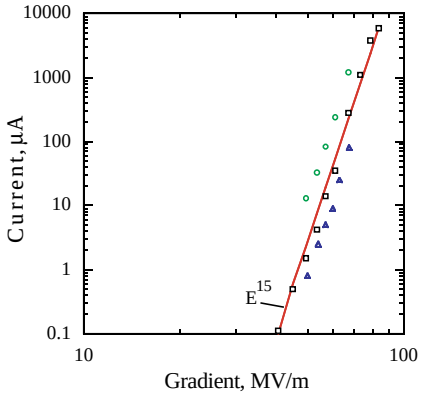

FIG. 30. Dark currents from an NLC prototype cavity.

Measurements of x ray fluxes and energies in a superconducting cavity in the CESR storage ring have been made at Cornell to evaluate the feasibility of single particle detectors in the region of the cavities [28]. In this measurement the x ray detector was placed at some distance from the cavity and did not view the emitting surfaces directly. Nevertheless, as shown by the data in Fig. 31, an E^{20} dependence on accelerating voltage again implies that Fowler Nordheim dark current electrons are the dominant process. In this experiment, as in measurement of the Taiwan photoinjector gun, the photon energy was measured, showing a wide spectrum with a geometric mean energy of about 100 keV.

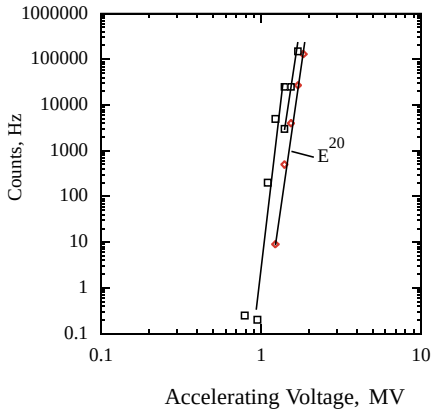

FIG. 31. X ray fluxes from an rf cavity.

We have also examined data on radiation levels and cavity breakdown which was taken during the tuneup of the Fermilab Linac upgrade [29]. This data was collected systematically during the operational life of this linac. Data from the conditioning period of the Fermilab 805 MHz linac upgrade show that the sparking rate is strongly correlated with the radiation level measured near the cavities as shown in Fig. 32. This data incorporates both periods of conditioning, when the cavity field levels were being increased, and normal operating conditions, when the cavity field were fairly stable. The raw sparking rate is seen to be directly proportional to the radiation level, implying that the two effects are related. The causal relation involved here is not well understood.

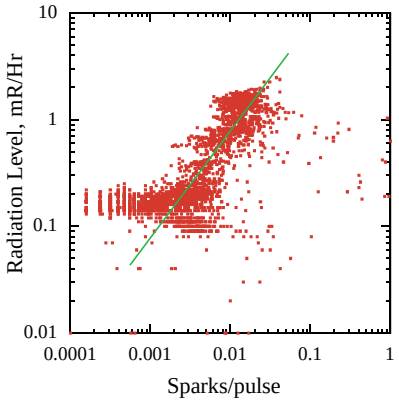

FIG. 32. Fermilab linac data.

V. THE PHYSICS OF EMITTERS

We are interested in a number of issues, such as how emitters are activated, how one can deactiveate them or minimize their effects and how dark current emission is related to breakdown. Unfortunately, this data provides only indirect information on the nature of the emitters. We describe how our data are sensitive to a variety of phenomena.

We define the exponent of the emission law as

$$n = \frac{E}{I}\frac{dI}{dE},$$

with I and E as the current and field. It is possible to derive information about β_{FN}, and other parameters, directly from knowledge of the exponential dependence of dark currents or x ray fluxes. This $I \propto E^n$ dependence is shown in Fig. 33. Measurements with current transformers or radiation monitors outside the shielding give values of $n \sim 9.6$ corresponding to high currents. Radiation monitors inside the shielding give values $n \sim 15$ and measurements which count individual photons and are sensitive to small currents give $n \geq 20$. This can be explained by the fact that more sensitive instrumentation see the threshold where the exponent is higher, and less sensitive instrumentation see higher currents produced where the field emission curve becomes flatter.

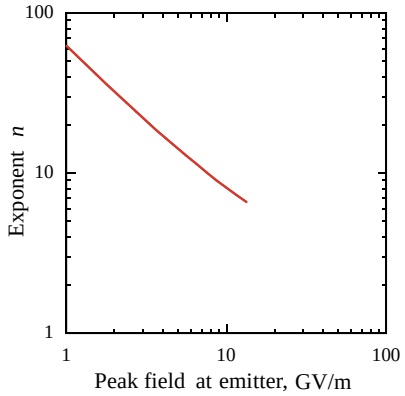

FIG. 33. Exponental dependence of field emission.

It is possible to estimate the order of magnitude of the current per emitter from the total current and the density of emitters as determined from the beam profiles, seen in Fig. 9. Using an emitter current of 10 mA, and a density of 10^5 emitters/meter^2, one obtains an average current of 3.5×10^{-6} A/emitter, assuming all emitters are roughly comparable.

A. The Correction for Sinusoidal Fields, A_{rf}

The Fowler Nordheim parameterization assumes that the electric field is constant, whereas it is actually varying sinusoidally. We have shown that the actual pulse of current only appears for about one tenth of the rf period. Since the current can be approximated by E^n, the integral can be evaluated numerically and

$$A_{rf} = \frac{1}{\phi}\int sin^n\phi \; d\phi \sim 0.1,$$

when evaluated over many cycles (and only positive polarities) has the dependence shown in Fig. 34. This issue has also been considered in a more detailed way, producing a more complicated expression for the Fowler Nordheim process [30] [31]. The $A_{rf} \propto E^{0.5}$ dependence is a small correction to the measured E^n values and systematic errors.

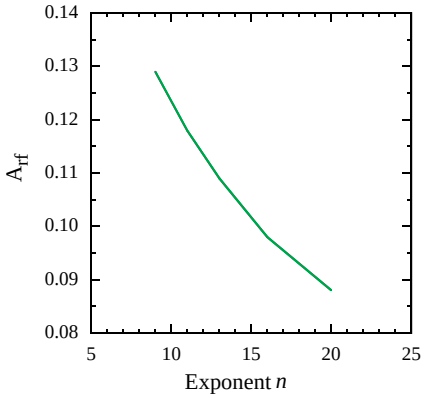

FIG. 34. Dependence of the rf correction factor.

B. Mechanical Properties

An active field emitter interacts with very high electric fields, almost independent of the emitted current, since measurable currents require electric fields at the tip of the emitter of $E = \beta_{FN}E_{acc} \sim 4 - 10$ GV/m. This produces high current densities, local heating and enormous forces, which act on the tiny tip of an emitter. The mechanical tension induced by an electric field is given by $T = 0.5\epsilon_0 E^2$, which gives pressures in the range of -380 MPa ($\sim$ 40,000 lb/in^2). This is equal to the tensile strength of copper. In principle, this could produce an unstable equilibrium, since sharp points would tend to deform to become sharper. As they become sharper, the joule heating and temperature increases, making deformations easier. The primary mechanical limit would be when the tips snapped off. The lowest values of the exponent n seen are ~ 9, comparable to the tensile strength of work hardened copper, and these are compatible with a surface field of 8 GV/m. This is significantly above the 10000 lb/in^2 stress at which soft annealed copper will begin to deform. More conservatively operated cavities run at values of $n \sim 14$, corresponding to a gradient of 5 GV/m and a tensile stress of 12,000 lb/in^2, after having been conditioned at higher fields. This is shown in Fig. 35. When installed, cavities should be dead soft,

but stresses of this magnitude would locally work harden them, as shown in Fig. 35 and Table II. Conditioning, which seems to operate at surface stresses comparable to the maximum strength of copper, may thus consist of simply tearing off all the sharpest emitting surfaces.

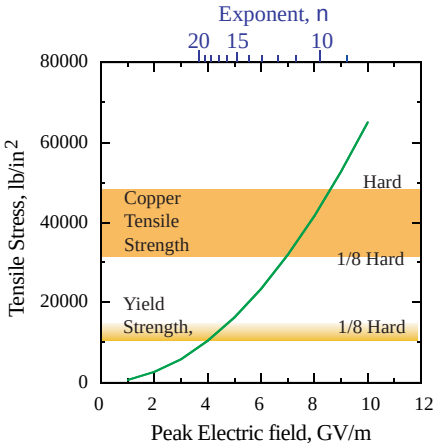

FIG. 35. Stress at emitters as a function of local field E and the exponent n.

Table II, Pressure on emitter surfaces.

Structure	n	E, GV/m	$-P$, MPa
This Exp	9.0 - 30	2.2 - 9.4	21 - 391
ANL/Taiwan	9.6	8.60	327
ISIS	13.5 - 14.0	5.50 - 5.75	134 - 146
IPNS	14.0	5.50	134
NLC prototype	15.0	5.05	113
CESR SCRF	20.0	3.60	57

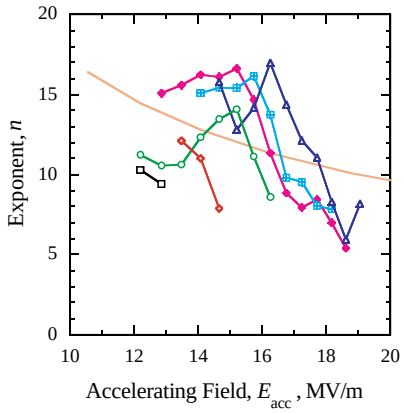

FIG. 36. Experimental values of $n(E_{acc})$ during conditioning. The smooth curve corresponds to the line in Fig 33.

Data during initial conditioning show the dependence of measured values of $n(E_{acc})$ calculated from $I(E_{acc})$. These data, Fig 36, show that n values are in the range 9 to 15 at lower gradients, but they decline rapidly as the field is increased. Part of the decline seems to be a function of space charge and other saturation effects discussed below.

The mechanical stress exerted by the electric field on the point of an emitter should be also sufficient to bend and move objects so that an emitter tip is perpendicular to the plane of the local surface of the structure, or weld particles to the surface [1]. This could be one mechanism for activating emitters.

The thermal behavior of an emitter depends on its geometry. For an emitter with an essentially conical geometry, where all currents are radial, the thermal behavior is comparatively simple. On the other hand, Padamsee and others have shown that many (if not most) emitters tend to be objects which sit on the surface of the structure, and may not be strongly coupled thermally to the body of the cavity [1]. These complex geometries are more difficult to model. In the case of a conical emitter the temperature has a roughly $1/r$ dependence, however, for currents of a few μA/emitter, the temperature would never become significant, even for emitter radii of less than 0.1 μm. On the other hand, if an emitter is part of an object sitting on the surface, the primary thermal loss would be by conduction to the body of the structure through a small contact point (at least at low temperatures) and much higher temperatures could be reached.

C. Chemical Effects

In addition to the Fowler Nordheim emission from points and thermal emission from hot surfaces, a variety of chemical effects may also be involved, Adsorbed gas has been associated with rf problems and vacuum perturbations have historically been associated with breakdown events in rf cavities, but the dark current emission seen here was not a major perturbation on the vacuum. Gas emission is more likely to be associated with absorption, rather than emission of dark currents.

Adsorbed gasses and radicals could contribute to emission of dark currents and breakdown. Various surface treatments which are capable of changing the surface chemistry are evidently able to change the dark current emission significantly, although we did not consciously alter the surface chemistry to look at these effects [2].

Other effects which could contribute to the emitter environment are chemical and structural changes in the material itself [10] [33]. Copper normally forms an oxide with very poor conductivity. It has been shown, however, that in the presence of high electric fields the surface can produce conducting filaments through the copper oxide effectively making a permanent breakdown channel [33]. This phenomenon is one example of a fairly general class of effects. The filaments are evidently formed by local thermal excursions which seem to permit changes in the atomic structure of the material. These filaments are closely related to similar phenomena in semiconductors. While emitting points could easily be eroded or destroyed, filaments inside the surface layers of the material might be much more robust. Unfortunately, these

phenomena were not experimentally accessible.

D. A Possible Mechanism for Emitter Formation

The strong electric fields can cause objects on the surface of the copper to align themselves perpendicular to the surface and interact with the field. Data from KEK show densities of $\sim$ 100 particles/cm^2 deposited on test silicon wafers, most of these particles had dimensions less than 1 μm [1]. We presume that the majority of this material is dielectric, primarily aluminum and silicon oxides, the primary constituents of the earth's crust. It has been shown that large quantities of finely ground rock, can be in the atmosphere. Wyoming, for example, has lost $\sim$200,000 km^3 of material by erosion over $\sim 2 \times 10^7$ years, a significant fraction of it by wind erosion [34]. Measurements at Saclay show that Al_2O_3 and SiO_2 particles on gold or niobium surfaces did not emit in DC fields but became strong field emitters in high gradient rf fields following dielectric heating, which would change their resistivity [35].

Once field emission has begun, breakdown at field emission sites will deposit much of the stored energy of the cavity locally in the copper, which could melt and eject liquid droplets which splash and make more and perhaps better, emitter sites. The electric field is sufficient to stand the copper filaments produced in splashes on end, making excellent emitter sites, but other mechanisms are also possible. The process of conditioning may then consist of ripping off the tops of the sharpest emitters.

E. Space Charge Effects

The dominant limitation on the emission of current from a surface is the Child-Langmuir limit, which gives the maximum current density, in A/m^2, as

$$j = 2.33 \times 10^{-6} V^{3/2}/d,$$

where V and d are the voltage and plate separation in a parallel plate geometry [20] [21]. In the case of a point emitter, this effect results in a $j \sim E^{3/2}$ dependence of the dark current. We have also looked at other effects to see if some information on the emitter geometry can be obtained from the beamlets produced by them. Examples of this behavior are shown in the data taken towards the end of the run on 12/1, (Fig. 14 and Fig. 37), which show that the experimental values of $n(E_{acc})$ decline rapidly to approach 3/2 somewhat asymptotically. The Dyke and Trolan data [12] shows a similar effect, (Fig. 38).

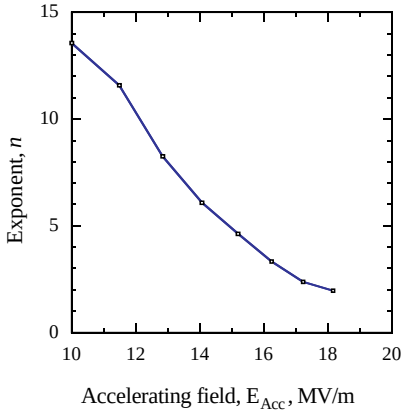

FIG. 37. A possible transition to space charge limited emission.

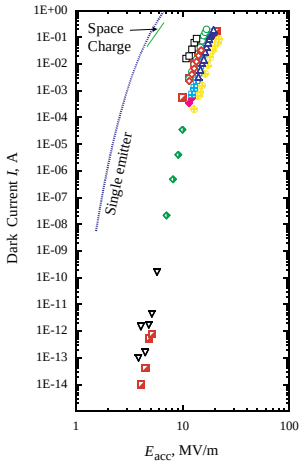

FIG. 38. Dark current measurements compared to current from a single tungsten emitter.

When the electrons are produced at the point of an emitter they become subject to space charge effects. Although the large electric fields accelerate the electrons quickly to high energies, space charge can be a significant effect near the surface. Space charge effects are parameterized by the perveance, defined by

$$K = \frac{I}{I_0}\frac{2}{\beta^3\gamma^3}(1-\gamma^2 f_e),$$

where I_0 is 17 kA, β and γ are the relativistic factors and f_e is the degree of charge neutralization. The subsequent evolution of the beam is governed by the relation

$$r/r_0 \sim 1 + 0.5K(z/r_0)^2,$$

where r_0 is the emitter radius. The electric field enhancement must be very local, and one would expect that space charge effects could be quite significant within a few mm of the surface before the electrons become relativistic.

This model should produce a dependence of the beamlet size on the current and source size like $r \sim I/r_0^2$, with the current strongly dependent on the electric field, and could give some evidence of the initial emitter size. Unfortunately, the emitter currents we see are physically quite small. By the time the beams have penetrated the titanium window the minimum size of all structure seen is about 100 μm. Simple arguments imply that space charge structure would be about 10 μm. or less.

Dyke and Trolan showed evidence of Child-Langmuir limits, and made a correction for image charges [12]. We looked for effects due to space charge limits, but again this was limited by the day to day repeatability of the system. The shape of the $I(E_{acc})$ we measured did not stay constant, and some days we saw some saturation of the curve at the highest currents which could be due to space charge effects probably due to changes in the surface. These effects were sometimes difficult to separate from changes in the pulse shape due to operation at higher gradients. We associated these effects with problems in conditioning and were not able to determine a clear relationship with space charge.

F. An "All Copper" Breakdown Model

Breakdown has been studied in terms of some of basic relations described by Kilpatrick [36]. The data from the tuneup of the Fermilab linac show that dark currents and breakdown seem to be related, but the mechanism is unclear. A particularly simple model, proposed by Dyke and Trolan, is that the tips of the field emitters get hot and break (vaporize or melt) forming a conducting path [12]. With the tungsten tips they used, this would require temperatures in the range of 3000 °C and currents greater than a few mA. Copper emitters would presumably arc at about 1/3 of this temperature. One set of data from Dyke and Trolan, Fig. 38, show that a single tungsten emitter can produce on the order of 0.5 A before breakdown occurs. At this current, space charge effects are significant.

While gasses are frequently assumed to be involved in breakdown, one can consider options which do not involve gasses. The data on dark currents during conditioning presented in Section III imply stresses near the tensile strength of the copper structure during conditioning. A straightforword assumption is that these emitter tips simply fracture and the copper fragments are propelled into the cavity. If this occured, the fracture line, both for the fragment and the solid structure, would probably also involve sharp corners which would produce subsequent fractures. The fragment would also be forced by electrostatic forces to align itself with the electric field, perhaps producing new and even larger forces on the copper, which would tear it into even smaller pieces. Breakdown could occur at lower fields due to metal fatigue and possible slow evolution of the mechanical structure of filaments and emitter sites. This is shown in Fig. 39.

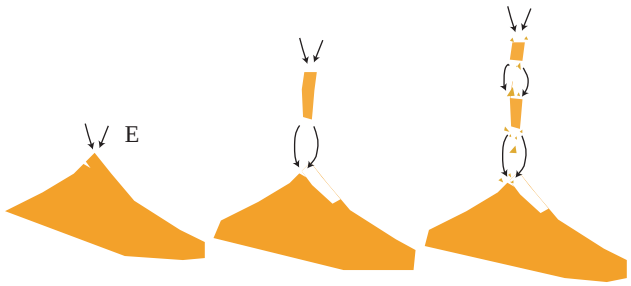

FIG. 39. Mechanical breakup of an emitter.

Dark current electrons would heat the fragment with a power equal to $P = IEx$ where I, E, and x are the current, electric field and gap distance. With currents a significant fraction of an Amp, and electric fields of 9 GV/m, large powers can be developed. In addition to these effects, the fragment would be expected to evaporate copper ions or ionized clusters, these ions and clusters should be accelerated into the cavity wall and further heat the original emitter site. This process has been described assuming a gas cloud above the emitter site [37], but an evaporating copper fragment would serve the same purpose. While adsorbed gasses would be involved in this process to some degree, the primary ions would be copper, as is seen experimentally [38].

While this mechanism is independent of cavity size or stored energy, the breakdown mechanism ultimately seems to deposit a significant fraction of the cavity stored energy locally at the breakdown site, ultimately in melted copper. The size of the stored energy then becomes the determining factor in the volume of copper that is melted.

VI. MINIMIZING DARK CURRENTS AND BREAKDOWN

There seem to be a number of methods of reducing dark currents in rf cavities. Making them cleaner by reducing adsorbed dirt has been shown to be essential in superconducting rf. Conditioning methods which clean the surface have been shown to be useful. Control of the surface structure with chemical polishing and different methods of turning also have been shown to have a significant effect [39]. The use of different materials may also be desirable, although there is less experimental evidence for this. There is a long history of improving the operation of superconducing cavities by eliminating field emitting particles contaminating the surface, and we would expect that similar effects could be obtained with copper surfaces. It is also possible that the surfaces could be made harder so that breakdowns could have less disruptive effects on the surface structure, however there is less experimental evidence to support this conclusion.

On the other hand, the construction of high gradient, low frequency cavities involves considerable stored energy and any breakdown event will deposit much of this energy in a small area of the surface. The subsequent evolution of the cavity probably is probably more dependent on the parameters of the breakdown event than on the treatment before breakdown. The limits of the control one has over the breakdown process with clean copper surfaces is not well understood.

VII. CONCLUSIONS

We have measured a number of parameters in a multicelled 805 MHz cavity and found that the data are consistent both with Fowler Nordheim field emission from small point sources, and with a variety of data taken in other accelerating structures which operate from 200 MHz to 11.4 GHz. Dark current emission seems to take place at local electric fields large enough to produce electrostatic forces sufficient to rip the copper emitters apart, a phenomenon which might be the trigger for breakdown events.

The data show the fluxes of dark currents emitted are too large for the present design of a single particle muon cooling experiment and we will have to look for ways of reducing this flux. There are a number of methods that have been developed during the development of high gradient superconducting rf systems and much of this technology should be applicable to this problem.

VIII. ACKNOWLEDGEMENTS

S. Geer, T. Kroc, A. Rowe and A. Tollestrup of FNAL, G. Drake and V. Stipp of ANL, R. A. Rimmer and M. Zisman of LBNL, S. Henderson of Cornell, Fermi Media services, Argonne Radiation Physics, J. Davis of Proxtronics Inc, Springfield VA, G. Lehr of Kodak, D. Errede of U of IL., R. Edgecock and D. J. S. Findlay of Rutherford Lab, C. Adolphsen and S. Tantawi of SLAC and E. McKigney of Imperial College and D. Kaplan and H. Li of IIT have been very helpful. The work was supported by Office of High Energy Physics of the US Department of Energy, the Illinois Board of Higher Education, the Illinois Dept. of Commerce and Community Affairs and the NSF.

---

[1] H. Padamsee, J, Knobloch, T. Hays, *RF Superconductivity for Accelerators*, John Wiley and Sons, Inc, New York, (1998)

[2] R. Latham ed., *High Voltage Vacuum Insulation*, Academic Press, London (1995)

[3] J. Norem, A. Moretti, M Popovic, Nucl. Instrum. and Meth. in Phys. Res. A 472 (2001) 600.

[4] V. Wu, *Design and Testing of a High Gradient RF Cavity for the Muon Collider*, PhD Thesis, University of Cincinati, Cincinati OH, (2002)

[5] A. Moretti, N. Holtkamp, T. Jurgens, Z. Qian, V. Wu *RF cavities for the Muon and Neutrino Factory Collaboration Study*, Proceedings of the XX International Linac Conference, Monteray CA, (2000).

[6] http://www.fnal.gov/projects/muon_collider/nu/study /report/machine_report/

[7] http://www.cap.bnl.gov/mumu/studyii /FS2-report.html

[8] C. M. Ankenbrandt et al. (Muon Collider Collaboration) Phys. Rev. ST Accel. Beams 2, 081001 (1999)

[9] M. A. Green, J. Y. Chen, S. T. Wang, *A Test of a Superconducting Solenoid for the MUCOOL RF Experiment*, IEEE Transactions on Applied Superconductivity 11, (2001), 2296

[10] R. V. Latham, *High Voltage Vacuum Insulation: The Physical Basis*, Academic Press, London, (1981)

[11] R. H. Fowler and L. Nordheim, Proc. Roy Soc **A119** 173 (1928)

[12] W. P. Dyke, and J. K. Trolan, Phys. Rev. **89** (1953) 799

[13] S. Dushman, Phys. Rev. 21(6), 623 (1923).

[14] Stangenes Industries, Palo Alto CA, USA.

[15] Tektronix Inc., Beaverton OR, USA.

[16] Perspective Scientific Limited, W1M 1LA, England.

[17] H. Enge, Rev. of Sci. Instr., 35, (1964), 278.

[18] H. A. Bethe and J Ashkin, *Passage of Radiations Through Matter*, in *Experimental Nuclear Physics* E. Segre, ed., John Wiley & Sons, Inc. New York, (1953).

[19] Hewlett-Packard, Palo Alto Ca,

[20] M Reiser, *Theory and Design of Charged Particle Beams*, John Wiley & Sons, Inc, New York, (1994).

[21] S. Humphries, *Charged Particle Beams*, Wiley, New York, (1990).

[22] W. P. Swanson, *Radiological Safety Aspects of the Operation of Electron Linear Accelerators*, IAEA Technical Reports Series No. 188, IAEA, Vienna, (1979)

[23] G. Shani, Radiation Dosimitry Instrumentation and Methods, CRC Press, Boca Raton, (1991).

[24] *TESLA, Technical Design Report, Part II, The Accelerator*, DESY 2001-011 (2001)

[25] D. J. S. Findlay, Rutherford Lab, Private Communication, (2002)

[26] V. Stipp, Argonne National Lab. Private Communication, (2002)

[27] C. Adolphsen, SLAC, Private Communication, (2002)

[28] S. Henderson, Cornell, Private Communication, (2001)

[29] T Kroc, Fermilab, Private Communication, (2001)

[30] J. W. Wang, *RF Properties of Periodic Accelerating structures for Linear Colliders* SLAC Report 339, Stanford Linear Accelerator Center, (1989)

[31] A. Chao, and M. Tigner *Handbook of Accelerator Physics and Engineering*, World Scientific, Singapore (1999), 391.

[32] Central Steel and Wire Company Catalogue, Central Steel and Wire Co, Chicago, IL, (2000).

[33] E. L. Cook, J. of Appl. Phys. **41**, 551, (1970).

[34] J. McPhee, *Rising From the Plains*, Farrar Straus &

Giroux, New York, (1986).
[35] B. Bonin, *Proceedings on the 6th Workshop on RF Superconductivity* R. M. Sundelin, ed, CEBAF, Newport News, Va, (1994).
[36] W. D. Kilpatrick, Rev. Sci. Instr. **28** (1952) 824.
[37] J. Knobloch, PhD Thesis, Cornell University, (1997).
[38] V. A. Dolgashev and S. Tantawi, *RF Breakdown in X-Band Waveguides*, in *Proceedings of the 9th International Workshop on Linear Colliders*, SLAC, Stanford CA, (2002).
[39] C. Suzuki, T. Kakanishi, S. Okumi, T. Gotou, K. Togawa, F. Furuta, K. Wada, T. Nishitani, M. Yamamoto, J. Watanabe, S. Kurahashi, H. Matsumoto, M. Yoshioka, K. Kogayakawa, Nucl. Instr. and Meth. in Phys. Res. A 462 (2001), 337.